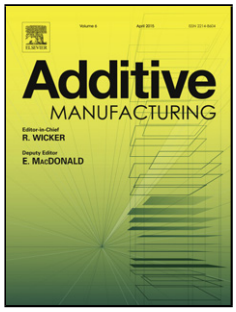

Title: An interlaboratory comparison of X-ray computed tomography measurement for texture and dimensional characterisation of additively manufactured parts

Authors: Andrew Townsend, Radu Racasan, Richard Leach, Nicola Senin, Adam Thompson, Andrew Ramsey, David Bate, Peter Woolliams, Stephen Brown, Liam Blunt

PII: S2214-8604(18)30333-6
DOI: https://doi.org/10.1016/j.addma.2018.08.013
Reference: ADDMA 471

To appear in:

Received date: 15-5-2018
Revised date: 19-7-2018
Accepted date: 9-8-2018

Please cite this article as: { https://doi.org/

An interlaboratory comparison of X-ray computed tomography measurement for texture and dimensional characterisation of additively manufactured parts

Andrew Townsend[1], Radu Racasan[1], Richard Leach[2], Nicola Senin[2,3], Adam Thompson[2], Andrew Ramsey[4], David Bate[4], Peter Woolliams[5], Stephen Brown[5], Liam Blunt[1]

[1]The Future Metrology Hub, University of Huddersfield, Huddersfield HD1 3DH, UK
[2]Manufacturing Metrology Team, Faculty of Engineering, University of Nottingham, Nottingham NG7 2RD, UK
[3]Department of Engineering, University of Perugia, Italy
[4]Nikon Metrology, UK, Ltd., Tring, Herts HP23 4JX, UK
[5]National Physical Laboratory, Teddington TW11 0LW, UK

E-mail: a.townsend@hud.ac.uk

Highlights
ISO 25178-2 surface texture from X-ray CT, interlaboratory comparison, is presented
Less than 0.5% *Sa* areal roughness between metrology CT and focus variation values
Artefact design allows separation of surface determination and scaling errors

Abstract

This paper presents the results of the CT-STARR (CT-Surface Texture for Additive Round Robin) Stage 1 interlaboratory comparison. The study compared the results obtained for the extraction of areal surface texture data per ISO 25178-2 from five X-ray computed tomography (CT) volume measurements from each of four laboratories. Two Ti6Al4V ELI (extra low interstitial) components were included in each of the CT acquisitions. The first component was an additively manufactured (AM) cube manufactured using an Arcam Q10 electron beam melting (EBM) machine. Surface texture data was extracted from CT scans of this part. The values of selected parameters per ISO 25178-2 are reported, including *Sa*, the arithmetic mean height, for which the values from the Nikon MCT 225 metrology CT measurements were all within 0.5% of the mean reference focus variation measurement. CT resolution requirements are discussed. The second component was a machined dimensional test artefact designed to facilitate independent analysis of CT global voxel scaling errors and surface determination errors. The results of mathematical global scaling and surface determination correction of the dimensional artefact data is reported. The dimensional test artefact errors for the XT H 225 commercial CT for length, outside diameter and inside diameter reduced from -0.27%, -0.83% and -0.54% respectively to less than 0.02% after performing mathematical correction. This work will assist the development of surface texture correction protocols, help define surface-from-CT measurement envelope

limits and provide valuable information for an expanded Stage 2 interlaboratory comparison, which will include a more diverse range of CT systems and technologies, further expanding the surface-from-CT knowledge base.

Keywords

ISO 25178, metrology, surface texture, additive manufacturing, X-ray computed tomography.

1 Introduction

Additive manufacturing (AM) methods enable the manufacture of components with complex external and internal geometrical features that cannot be manufactured using conventional subtractive techniques, such as grinding, milling or turning. However, measuring and characterising these features using conventional line-of-sight surface texture metrology instrumentation is challenging, if not impossible. Currently the principal method available for imaging the internal features of metal AM components is X-ray computed tomography (CT) [1]. CT has been used as an analysis tool for additive manufacturing technology in areas such as porosity [2-6] and dimensional metrology [7-9]. Until recently the only reported research detailing the extraction of surface information from CT was the extraction of profile data from lattice structures [10, 11]. Profile measurements are intrinsically two-dimensional in nature, with (*z*) heights being measured for (*x*) positional locations; however surface topography is three-dimensional and profile measurements are not able to fully characterise the actual surface. Optical areal surface measurement technologies are 2.5D measurements, with (*z*) heights for (*x,y*) measurement locations and so do include (*x,y*) spatial surface information. The importance of areal surface extraction from CT data has been discussed elsewhere [12, 13]. A novel methodology for the extraction of areal surface texture data per ISO 25178-2 [14] from metal AM components has been reported by the authors [15]. The results showed a -2.5% difference between the mean *Sa* value (arithmetic mean height) for the surface of an AlSi10Mg laser powder bed fusion (LPBF) AM component obtained when measured using CT compared to the same surface as measured using a standard surface metrology technique based on the focus variation (FV) principle. Further comparison work has also recently been reported by the authors [16, 17]. In this work measurements made using several optical systems as well as a CT system were examined. Previous work incorporating a dimensional test artefact in the CT scans of AM components had highlighted dimensional measurement scaling errors [15], so it was decided to include a dimensional test artefact in all the measurement scans reported here. The dimensional test artefact was designed to allow de-composition of the dimensional errors into global scaling errors and surface determination errors. Mathematical correction of the extracted dimensions for these two types of errors was performed to verify the validity of the de-composition technique. No corrections were applied to any of the surface texture measurements reported here; there is ongoing work in this field and the isolation and characterisation of global voxel scaling errors and surface determination errors provided by the analysis of a dimensional test artefact included within CT scans of AM surfaces will provide valuable information for the development of AM surface texture data correction protocols. Previous research by the authors into the extraction and characterisation of areal surface texture data from CT data was performed using aluminium AM surface and dimensional test artefacts [15]. The AM test artefact used in that research was manufactured

using a LPBF machine. The top (upskin) surface of the AM test artefact was used as the surface-of-interest. It is important that the techniques reported in the previous research be verified for other materials and surface conditions, therefore the raw material, manufacturing process and surface measurement location were all changed for the research reported here. A number of barriers must first be overcome in order for CT to be used in industrial settings. Particularly, an assessment is required of the ability of the technique to remain robust to a variety of materials and a range of machines with differing measurement techniques, envelope sizes and image resolutions. This has prompted the development of the interlaboratory comparison 'round robin' (RR) reported here [18]. Consideration was given to performing a global comparison involving many types of machines and, through necessity, allowing the participants to select their own set-up parameters and conditions. However, it was decided that a tightly controlled, smaller scale, geographically local RR would be a sensible initial approach. If no performance conclusions could be drawn from a tightly controlled RR, then there would be little scientific merit in an expanded study. Stage 1 of the RR included four participants using similar machines and similar scan measurement parameters. The Stage 1 RR was performed exclusively in the UK, in order to tightly control sample transportation, sample measurement and data analysis.

2 Methodology

This section consists of a description of the two measurement test artefacts and reference measurements (section 2.1); a list of RR participants, the CT machine types and the CT settings used (section 2.2); details of the data reconstruction process and dimensional data extraction (section 2.3); and a presentation of the surface data extraction and analysis sequence (section 2.4).

2.1 Measurement test artefacts

Two Ti6Al4V ELI (extra-low interstitial) test artefacts were included in all the scans performed: an AM surface test artefact, described in section 2.1.1 and a dimensional test artefact, described in section 2.1.2.

2.1.1 AM surface test artefact

The material chosen for the AM surface test artefact for this RR was Ti6Al4V ELI (Grade 23). Ti6Al4V ELI is widely used in the aerospace and medical industries. The RR AM test artefact was produced using the electron beam melting (EBM) process. The test artefact was manufactured on an ARCAM Q10 machine; the nominal powder size was (45-100) µm. A vertical (side) surface was chosen as the surface-of-interest for the RR measurements (see Fig. 1).

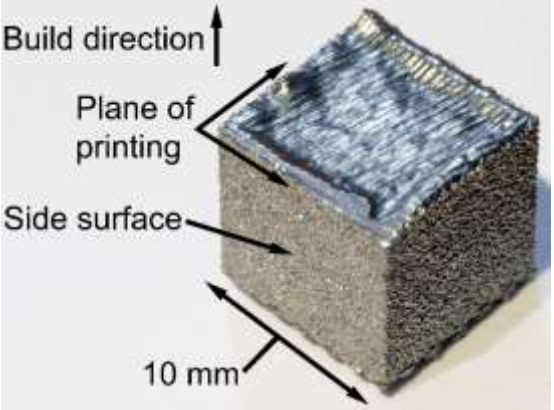

Fig. 1. Ti6Al4V ELI EBM AM test artefact.

The required surface measurement area, (8 × 8) mm, was derived from the profile roughness (*Ra* ≈ 30 µm), using Table 1 of ISO 4288 [19] (profile) and ISO 25178-3 [20] (areal) specification standards. The test artefact was a 10 mm per-side cube, similar to the size of the aluminium test artefact used in [15]. This design includes additional margin above the (8 × 8) mm required measurement area to avoid build edge effects and to allow for the required cropping of the extracted surface.

2.1.2 Dimensional test artefact

The dimensional test artefact included in each measurement was machined from Ti6Al4V ELI bar stock to provide similar X-ray attenuation properties as the Ti6Al4V ELI AM test artefact. The dimensional artefact was machined from bar stock and not manufactured using EBM AM because of the greater bar stock material homogeneity and lower probability of porosity, thus producing more consistent grey-scale values during the surface determination process (see section 2.3) and reducing the chance of local surface defects effecting coordinate measuring machine (CMM) and CT dimensional measurements. This dimensional test artefact included three measured dimensions: an outside diameter (OD) and an inside diameter (ID), both of approximately 3 mm, and a step-length defined by the perpendicular distance between two parallel surfaces separated by a step of approximately 4.5 mm (see Fig. 2). The dimensional test artefact was designed to allow discrimination between dimensional errors induced by voxel scaling and dimensional errors induced by surface determination. The ability to separate and quantify these two potentially significant, but very different, sources of error will provide data for independent systematic corrections. The artefact is similar in design to the dimensional test artefact used in [15].

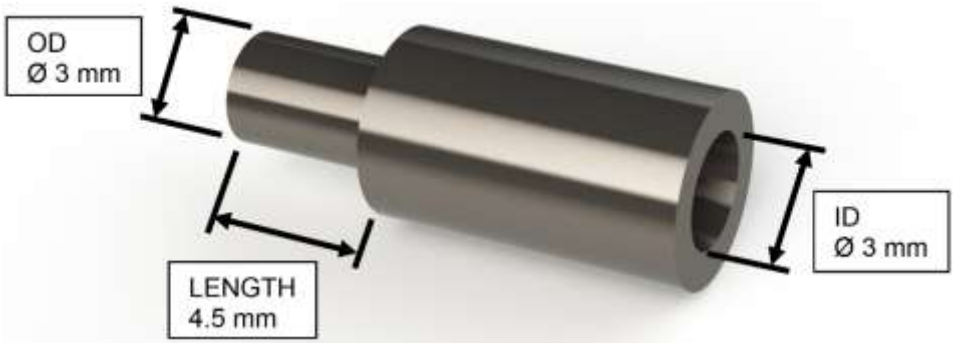

Fig. 2. CAD rendering of the dimensional test artefact.

Surface determination is the calculation of the surface position in the voxel volume reconstructed from the CT projections. The calculated position of the surface, at the transition between material (Ti6Al4V ELI) and background (air) is based on the grey-scale values of the volume voxels. Errors in determining the position of surfaces results in errors in the dimensional characterisation [21]. Voxel scaling errors, i.e. errors in defining the correct size of the voxels, also produce dimensional characterisation errors and thus different OD, ID and Length values for the test artefact. Because of the geometry of the test artefact, and the targeted dimensions (OD, ID and Length), dimensional errors induced by voxel scaling and surface determination can be discriminated. A voxel scaling error produces similar changes in the surfaces responsible for the OD, ID and Length values: for example: larger voxels will always lead to larger dimensions. Surface determination error will lead to contrasting effects. For example, if surface determination were to place the computed surface uniformly away from the “material” of the part, toward the background (air), then the calculated OD would be oversized, the ID would be undersized and the step-length would not change, as the surfaces are parallel and facing the same direction. Once the two error types are discriminated, mathematical corrections may be applied to the extracted component dimensions. Fig. 3(a) is a representation of the effect of correcting for voxel scaling error, in this example correcting for oversized voxels that have resulted in a reconstructed component with an oversized OD, ID and length. The resulting correction reduces the OD, ID and length. Fig. 3(b) shows the effect of correcting for a surface determination error that has computed the material surface beyond the actual surface (toward the background (air)). The correction in this example is equivalent to figuratively “removing” surface, therefore reducing the OD, increasing the ID and not altering the step-face length dimension. The evaluation, discrimination and correction process applied to the measured artefact is detailed in section 3.2.3.

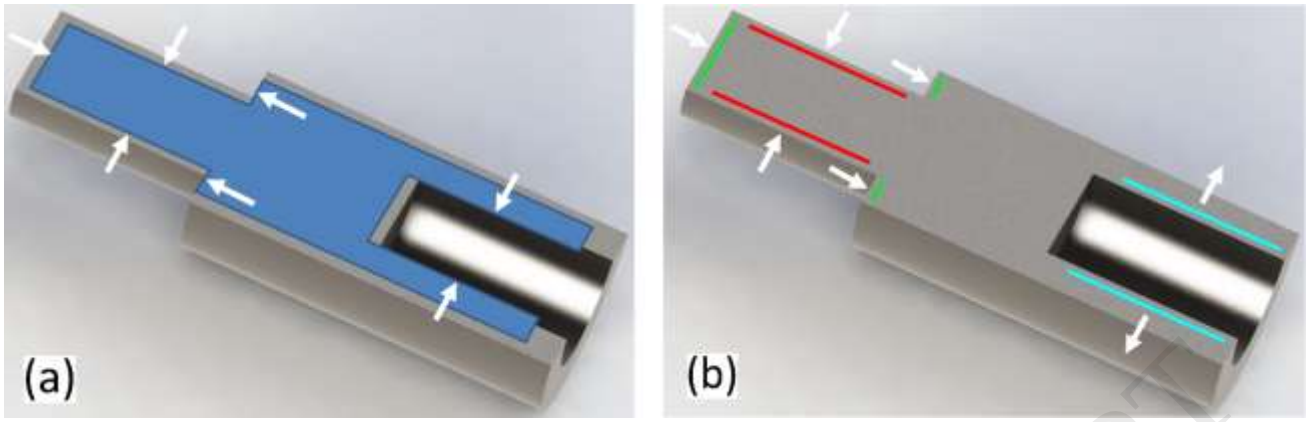

Fig. 3. Examples of the mathematical corrections applied to the dimensional artefact.
(a) correction for the CT voxels being oversized (OD, ID and Length all reduced),
(b) correction for the surface determination computing the surface location beyond the actual surface (OD reduced, ID increased and Length unchanged).

2.1.3 Reference measurements

The AM surface test artefact and dimensional test artefact were measured using an Alicona G4 focus variation instrument and a Zeiss Prismo CMM respectively prior to the RR.

For the surface texture measurements, the authors have chosen to use focus variation as the reference, primarily because it has higher lateral and vertical resolution than the CT systems, but also because it has been shown to produce satisfactory results in previous work with AM surfaces [15, 16, 22, 23]. Five reference surface measurements were taken of the same region of the AM surface artefact using the Alicona G4 with a 10× objective lens installed. Lateral sampling distance was 2.33 µm, with a vertical resolution of 0.5 µm.

Ten reference measurements of OD, ID and Length (thirty measurements total) were made of the dimensional artefact using a Zeiss Prismo CMM, following the same protocol the authors used in [15]. The dimensional artefact was not removed from the fixture between CMM measurements. The CMM maximum permissible error (MPE) is (1.9 + L/300) µm (L in mm). CMM scanning mode was used whereby the probe tip traverses the surface, remaining in contact with the surface. A 1.0 mm diameter ruby probe tip was used for all measurements. The ID and OD were measured at four locations along the length of the artefact; measurements were taken at distances 0.5 mm, 1.25 mm, 2.0 mm and 2.75 mm from the respective end faces (see Fig. 4**Error! Reference source not found.**). 100 measurement points were made per circle and 100 points were made on each of the two surfaces comprising the step-face surfaces. The reported OD and ID values were extracted from total least squares cylinders fitted to the data sets. Similarly, the Length values were generated from the distance (at the central axis of the dimensional artefact) between total least squares planes fitted to the step-length face data sets.

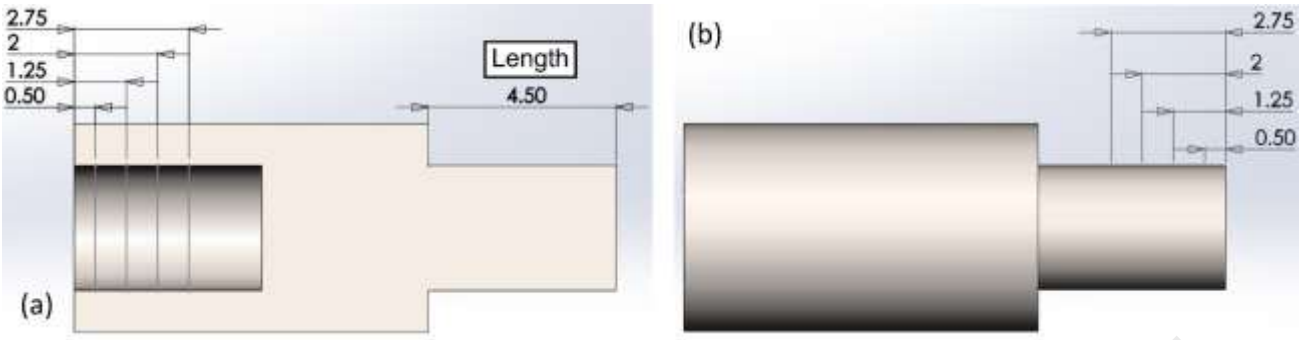

Fig. 4. Location of CMM measurements. (a) ID and Length, (b) OD. All dimensions in mm.

For CT measurement, the AM surface artefact and the dimensional test artefact were then mounted within an Acrylonitrile-Butadiene-Styrene (ABS) AM fixture. The fixture was manufactured from a material with significantly lower density and X-ray attenuation coefficient than the test artefacts to minimise the effect of X-ray attenuation through the fixture at the energies required to fully penetrate the Ti6Al4V ELI test artefacts. The fixture was designed to maintain an air-gap between all measured surfaces and the fixture. This fixture was designed as such to avoid possible errors in surface determination computation (see section 2.3) that may be caused by local ABS–Ti contact and by local three-material ABS–Ti–air interfaces. Surface determination is based on voxel grey-scale value, and local areas with surfaces generated after evaluation of the grey-scale values of ABS–Ti and ABS–Ti–air may not be consistent with surfaces generated at the Ti–air interface and may subsequently influence the values of extracted surface texture parameters and dimensions. The air-gap ensures a (reproducible) universal two-material interface. The AM artefact measurement surface was angled at 45° to the horizontal and positioned to minimise CT-generated ring and cone-beam artefacts [24]. The two artefacts were positioned so there was no projection overlap during the scans. The fixture development process is reported elsewhere [18]. A CAD section view of the assembly is shown in Fig. 5. The test artefacts were not removed from the fixture at any time during the complete set of RR measurements.

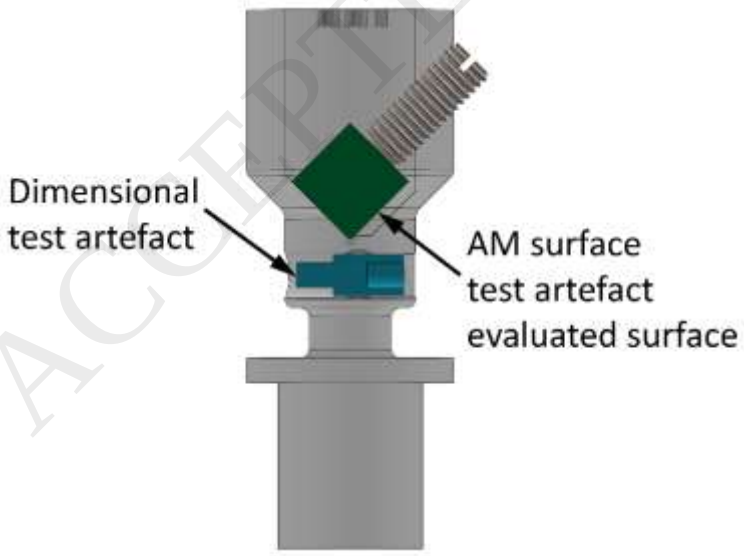

Fig. 5. CAD section view of the test artefacts within the fixture.

2.2 Round robin participants and CT measurement settings

There were four RR participant laboratories: the University of Huddersfield, the University of Nottingham, the National Physical Laboratory (NPL) and Nikon Metrology. To reduce the number of process variables, all participants utilised a Nikon CT machine: three used the MCT225 metrology CT and one used the XT H 225 industrial CT. The settings for the three Nikon MCT225 systems are shown in Table 1; the CT settings for the Nikon XT H 225 system are shown in Table 2. Measurement settings were selected to optimise the exposure contrast while maintaining a fully-focussed X-ray beam; as the power into the electron-generation filament is increased beyond 10 W the electron beam striking the tungsten target is progressively de-focussed to maintain the energy per unit area at safe levels. The X-ray beam generated at the target subsequently becomes more de-focussed as the electron beam is de-focussed. All measurements were performed with power levels maintained below 10 W, therefore maintaining a fully focussed electron and X-ray beam.

Table 1. Nikon MCT225 measurement settings.

Parameter	Value	Parameter	Value
Filter material	Copper	Exposure time	2829 ms
Filter thickness	1.0 mm	Voxel size (length of one side of voxel cube)	8.7 µm
Acceleration voltage	160 kV	Number of projections	3142
Filament current	62 µA	Detector size (pixels)	2000 x 2000

Table 2. Nikon XT H 225 measurement settings.

Parameter	Value	Parameter	Value
Filter material	Copper	Exposure time	2829 ms
Filter thickness	1.0 mm	Voxel size (length of one side of voxel cube)	17.3 µm
Acceleration voltage	160 kV	Number of projections	1583
Filament current	62 µA	Detector size (pixels)	1008 x 1008

The most obvious differences between the settings of the two CT systems are the voxel size and the number of projections used: for the MCT225 these were 8.7 µm and 3142 respectively, compared to 17.3 µm and 1583 respectively for the XT H 225. Voxel sizes are the length of one side of the voxel cube. The difference in voxel size is primarily due to the different pixel densities at the detector (2000 × 2000 pixels for the MCT225, 1008 × 1008 for the XT H 225). The effect of measurement voxel size on the extracted surface texture parameters is discussed in section 3.3. Future work will include investigation of the effect that the number of projections has on the extracted surface texture parameters. Five measurements were made on each CT system. The test artefacts were not disturbed between each of the measurements and the fixture was not removed from the stage, as removing and replacing the test artefacts from the fixture would have increased the probability of component damage during the RR process. The AM test artefact was removed and replaced during the initial process analysis [15] and there were no observed differences in the extracted areal surface data between measurement sets. The test artefact assembly (i.e. the assembly comprised of the dimensional test artefact, the surface test artefact and the fixture), mounted in the Nikon XT H 225, is shown in Fig. 6(a).

The test artefact assembly mounted in the Nikon MCT225 is shown in Fig. 6(b). The 1 mm copper filter, included to reduce the effects of X-ray beam hardening and to reduce the image contrast, can be seen in front of the X-ray windows.

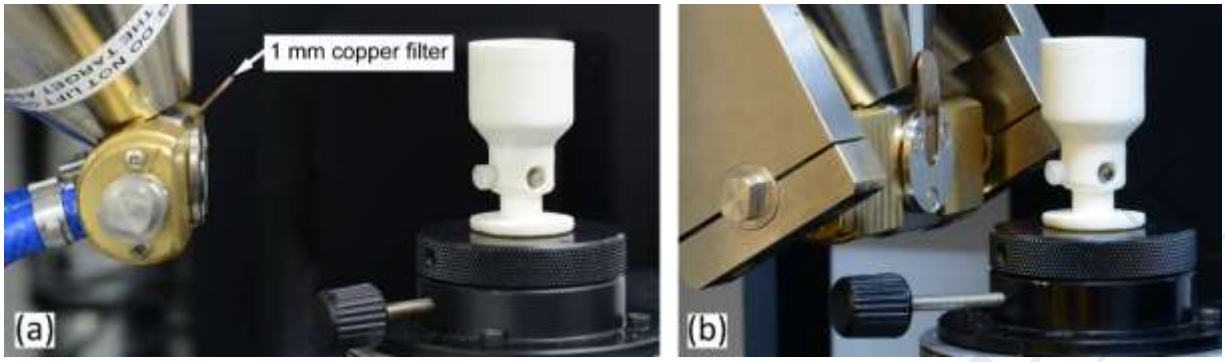

Fig. 6. Test artefact assembly mounted in the measurement position.
(a) Nikon XT H 225, (b) Nikon MCT225.

2.3 CT reconstruction and dimensional data extraction

All the reconstruction, surface analysis and parameter extraction steps were performed by the first author in order to reduce variability. Reconstruction was performed using Nikon CT Pro 3D [25]. Local iterative surface determination was performed using VGStudio MAX 3.0 [26] using the maximum gradient method, starting from the ISO50 surface and with a search distance of 4.0 voxels. A volume from the body of the dimensional artefact was selected as the “material” and a volume from the 3 mm diameter cavity of the same artefact was selected as the background for generation of the ISO50 surface. After performing surface determination, two regions of interest (ROI) were extracted: a section of the AM test artefact including the AM surface-of-interest and the complete dimensional test artefact. The dimensional test artefact was converted to STL file format using the VGStudio Max 3.0 “Normal” setting and the AM surface ROI was converted to PLY format using the “Super Precise” setting. The “Normal” setting was used for the dimensional artefact as the dimensional analysis of this artefact does not require the higher resolution of the “Super Precise” setting used for surface analysis of the AM component. Processing time is less and the generated file sizes are smaller using the “Normal” setting. The reported OD and ID values from the CT dimensional test artefact measurements were extracted from total least squares cylinders fitted to the STL data set points for the OD and ID surfaces located between 0.5 mm and 2.75 mm from the artefact end faces (dimensions as shown in Fig. 4). The Length values were generated from the distance (at the central axis of the dimensional artefact) between total least squares planes fitted to the step-length face CT data sets.

2.4 AM surface data processing sequence

Before texture parameters can be computed on the FV an CT measured surfaces, some data processing is necessary to ensure all the measured datasets refer to exactly the same portion of topography (as the presence/absence of even a few topographic formations in some datasets only, may alter the texture

parameter results). In order to ensure that the datasets refer to the same portion of topography, they need to be aligned first (with rotation and translation in 6 degrees-of-freedom), and then cropped to exactly the same boundaries. Alignment in turn requires the native height maps produced by the FV process be exported from the Alicona G4 software package as triangle meshes before they can be translated and rotated. Similarly, the CT datasets may be exported as triangle meshes. Once aligned, triangle meshes need to be converted into height map format, as the latter is the format needed for computing texture parameters. The entire sequence of operations performed for post-processing and texture parameter computation is summarised in Fig. 7, and involves both custom-computation steps and the use of commercially available software. The steps are described in detail in this section.

Extraction of the initial datasets

From CT volumetric data, a ROI was extracted containing the entire (10 × 10) mm surface of interest and portions of the adjacent four sides (Fig. 7, step (1)). The FV measurement included the entire surface of interest. To remove the edges and any trace of the side surfaces, both datasets were cropped using Meshlab [27].

Conversion to PLY mesh format

The FV datasets, initially saved in the STL format, were converted to PLY format in Meshlab. The PLY file format mesh data contains vertex and face information without repetition of shared vertices resulting in approximately one third the size of STL format files, so reducing storage requirements and computation time. The conversion from STL to PLY is a lossless process as vertex co-ordinate data is unchanged (see Fig. 7, step (2)). The CT surface data were exported from VGStudio MAX 3.0 as triangle meshes, directly in the PLY format.

Surface alignment

One of the FV measurements was chosen arbitrarily as a master for the alignment and further cropping of all other data sets. The master was not trimmed and so remained larger than the other surfaces. This was done to allow the maximum area of the measurement sets to be used for the alignment process. Iterative closest point (ICP) alignment, implemented in CloudCompare [28], was performed between each of the PLY data sets (CT and FV) and the master. The RMS distance between the points belonging to the two aligned datasets was used to evaluate alignment quality. A threshold on the minimum improvement of such value was set to 5×10^{-5} mm and used as termination criterion for the ICP procedure (see Fig. 7, step (3)).

Triangulated mesh cropping to (8.4 × 8.4) mm

Once alignment was complete, each of the aligned surfaces was cropped to a size of approximately (8.4 × 8.4) mm, by triangle removal, in CloudCompare. The cropping coordinates were based on the coordinate system of the master FV file, so ensuring the same area was cropped for all samples (Fig.

7, step (4)). This cropping may not result in straight mesh boundary edges because of non-controllable positioning of the triangles. For this reason cropping to final target size of (8 × 8) mm was performed on height map data (see later steps).

Conversion to height map format

CT triangle meshes are true 3D (*x,y,z*), which may contain undercuts and re-entrant features. Converting the CT data to height map format is required for the generation of surface texture parameter data per ISO 25178-2. Height map format consists of (*z*) height values within an (*x,y*) matrix. Errors can occur during this mesh-to-height map conversion process if the data to be converted has more than one (*z*) value at any one matrix location, such as is the case with re-entrant features. The CT triangle meshes were therefore "cleaned" in Meshlab by pre-emptive elimination of negatively oriented triangles and triangles covered by others according to the reference line-of-sight, as established by the master FV measurement (see Fig. 7, step (5)). After triangle elimination, any isoated vertices in the CT data sets (i.e. vertices non associated to any triangles) were removed, again in Meshlab. Finally, the conversion into height map format (for the CT and FV mesh data sets) was performed by a custom procedure implemented in Matlab [29], where the vertices were extracted from the triangle mesh and used to implement a bilinear interpolator for computing height at any location (Fig. 7, step (6)). Potential interpolation problems with the CT data sets due to undercuts and re-entrant features were eliminated by the previous triangle deletion operations. The interpolator was interrogated at multiple (*x,y*) positions organised as a regular grid with 2.5 µm spacing to obtain height maps. The final height maps were saved in the SDF format [30] for use in any surface metrology software.

Cropping height map to (8 × 8) mm

The height map data was then cropped to (8 × 8) mm (to comply with the requirements of ISO 25178-3, which suggests the sizes of the datasets to be used for computing texture parameters). Cropping was implemented in Matlab (see Fig. 7, step (7)).

Filtering per ISO 25178-3

Levelling (least squares) and filtering were then performed. A Gaussian regression L-filter nesting index of 8 mm and an S-filter nesting index of 0.025 mm per ISO 25178-3 were then applied to all surfaces, implemented in SurfStand [31] (see Fig. 7, step (8)).

ISO 25178-2 parameter generation

ISO 25178-2 areal texture paramters were generated from each surface for comparison using SurfStand (see Fig. 7, step (9)).

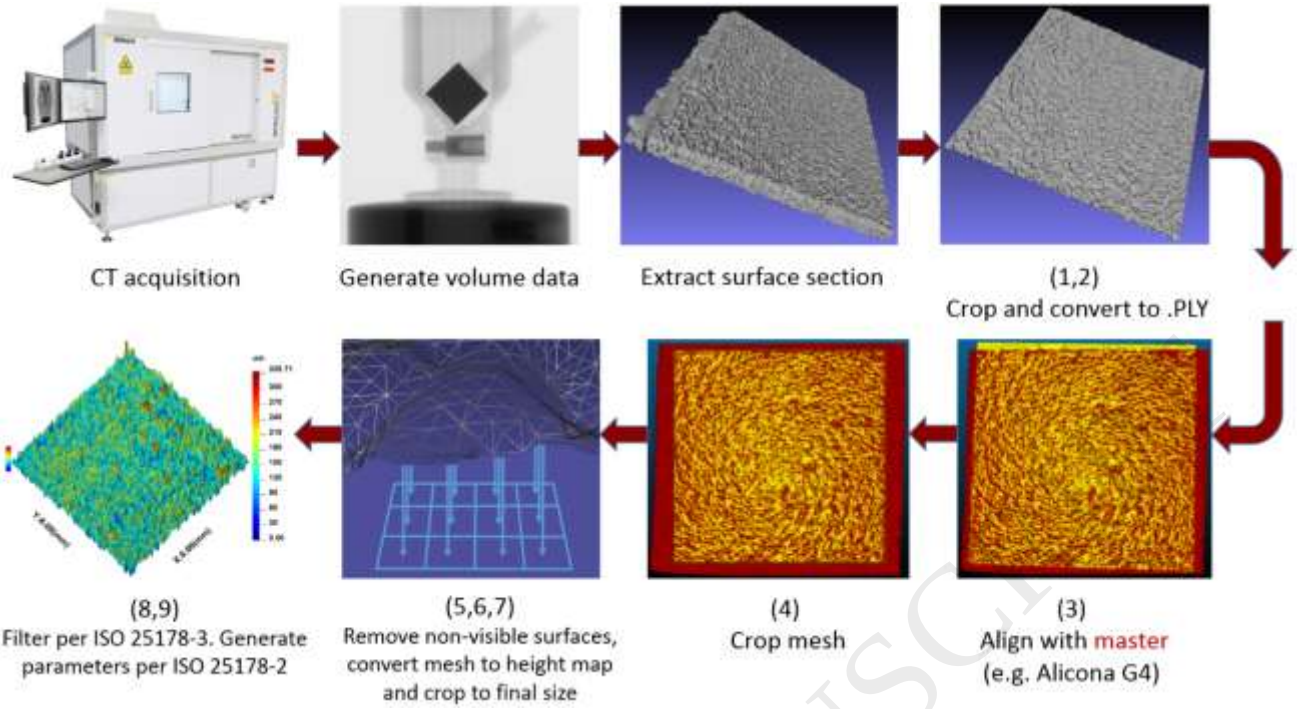

Fig. 7. CT surface measurement and characterisation sequence.
Sequence numbers in parentheses are listed in the individual steps of section 2.4.1.

3 Results and discussion

3.1 Areal texture parameters

The results for selected ISO 25178-2 surface texture parameters, computed on the reference FV datasets and the CT datasets, are reported in Table 3. As parameters were calculated on five regions, results are reported as sample mean values and standard deviations (SD). The ISO 25178-2 parameters reported in Table 3 were chosen because of their proven sensitivity to variation of manufacturing process parameters in AM surfaces [13]. The CT results are from the Nikon XT H 225 industrial CT (XTH) and the three Nikon MCT225 metrology machines (MCTA, MCTB, MCTC). The percentage differences between the CT mean values with respect to the FV mean values are shown in Table 4.

Table 3. Surface texture parameter mean values and sample standard deviation.

Parameter	Mean FV	SD FV	Mean XTH	SD XTH	Mean MCTA	SD MCTA	Mean MCTB	SD MCTB	Mean MCTC	SD MCTC
Sa / µm	25.5	0.001	24.1	0.027	25.5	0.011	25.5	0.019	25.6	0.006
Sq / µm	32.6	0.002	30.9	0.032	32.5	0.009	32.5	0.023	32.6	0.007
Sz / µm	335.3	0.199	324.0	2.941	335.2	1.244	334.2	1.423	335.4	2.332
Ssk	0.26	<0.001	0.08	0.015	0.20	0.001	0.21	0.001	0.21	0.001
Sku	3.7	<0.001	3.7	0.010	3.6	0.004	3.6	0.005	3.6	0.003
Sdr (%)	40.2	0.014	28.3	0.131	41.9	0.117	42.4	0.137	43.8	0.103

Table 4. Differences between texture parameter mean values.

Parameter	Difference between mean XCT and FV values			
	XTH	MCTA	MCTB	MCTC
Sa / µm	-5.2%	0.2%	0.3%	0.5%
Sq / µm	-5.2%	-0.1%	-0.1%	0.2%
Sz / µm	-3.4%	0.0%	-0.3%	0.1%
Ssk (absolute)	-0.2	-0.1	0.0	0.0
Sku	-2.0%	-2.9%	-3.1%	-3.1%
Sdr (%) (absolute)	-12.0	1.7	2.2	3.5

Comparing the differences between the CT measurements and the FV measurements for the two types of machines shows the MCT225 difference values for *Sa*, *Sq* and *Sz* parameters are approximately an order of magnitude less than those for the XT H 225. For example, the difference between the MCTC mean *Sa* value and the mean FV value is 0.5%; the difference between the XTH 225 mean *Sa* value and the mean FV value is 5.2%. Fig. 8 shows the false colour height maps for one FV measurement and one MCT225 measurement from the MCTC set. It is difficult to visually differentiate between the two height maps. Fig. 9 shows the confidence intervals (CIs) of the means of *Sa*, *Sq* and *Sz* for all machines, computed at 95% confidence level. The results indicate that the parameters computed on the XTH datasets are the most significantly different from the others.

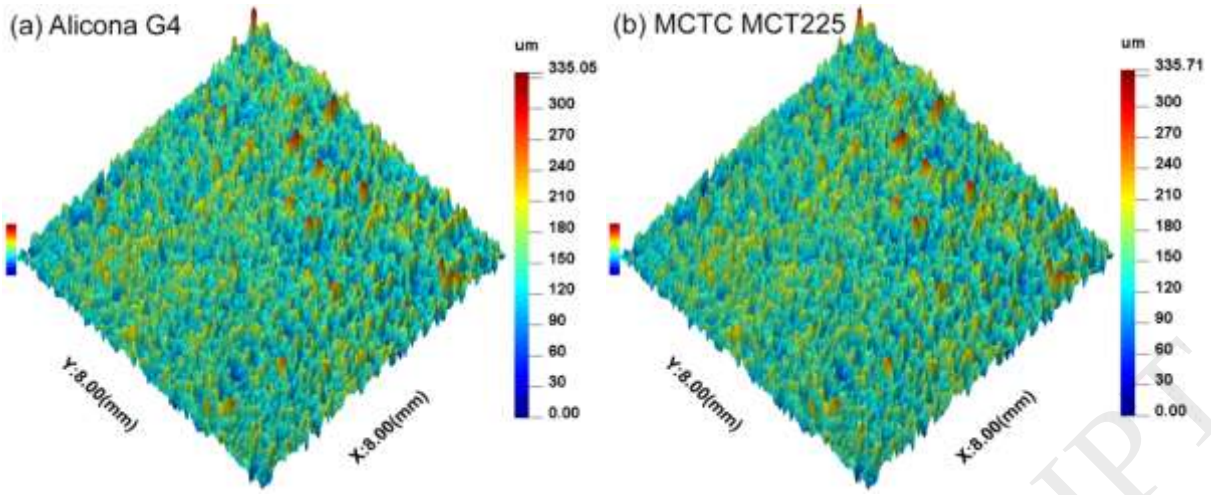

Fig. 8. False colour height maps. (a) FV, (b) MCTC.

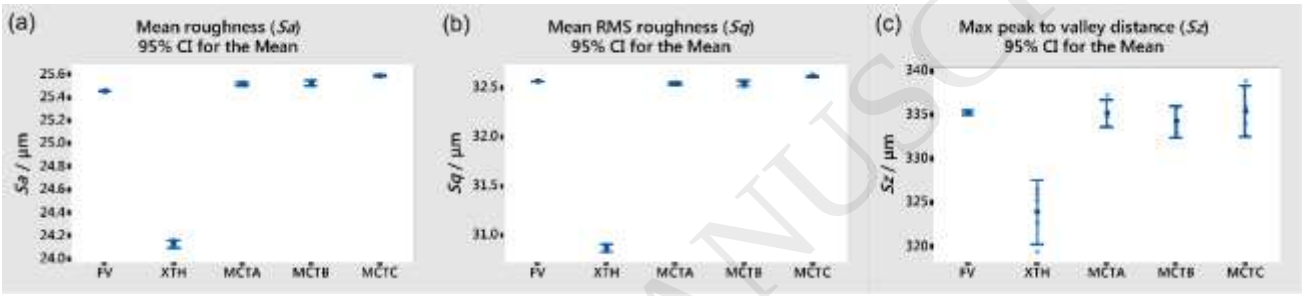

Fig. 9. Surface texture results. (a) *Sa*, (b) *Sq*, (c) *Sz*.

3.2 Dimensional test artefact

3.2.1 Measurement MPE values

The Nikon MCT225 metrology CT and Zeiss Prismo CMM have maximum permissible error (MPE) values as follows, as specified by the manufacturer:

Nikon MCT225 MPE: ± (9 + L/50) µm. (L in mm).
Zeiss Prismo CMM MPE: ± (1.9 + L/300) µm. (L in mm).

The CT reduced MPE limits displayed on the charts that follow are the CT manufacturer's MPE limits reduced by the value of the CMM MPE limit. This tightening of the CT MPE limits allows for the fact that the actual component dimension may be anywhere within the MPE limit range of the CMM reported value. This tightening means that all measurements displayed within the CT reduced MPE limits will be within (9 + L/50) µm of the actual dimension. This is similar to the reduction of a component allowable tolerance based on the inspection instrument accuracy [32].

The MPE limits are shown in figures 10-12 as follows:

CMM MPE limits.

CT reduced MPE limits.

3.2.2 Measurement results

The dimensional results for the CMM and the CT measurement sets are shown in Table 5. The percentage difference of the CT measurement results with respect to (wrt) the CMM reference measurements are shown in parentheses. The sample standard deviations for all CT measurement sets, including the XT H 225 industrial CT measurements, are all less than 1.5 µm, showing excellent repeatability for all measurements.

Table 5. Dimensional test artefact mean and standard deviation results.

Measurement method	Mean length (mm) [% dif. wrt CMM]	Sample std. dev. (mm)	Mean OD (mm) [% dif. wrt CMM]	Sample std. dev. (mm)	Mean ID (mm) [% dif. wrt CMM]	Sample std. dev. (mm)
CMM (10 meas.)	4.6240	<0.00005	2.9735	0.00005	2.9846	0.00005
XTH (5 meas.)	4.5992 [-0.54%]	0.0008	2.9655 [-0.27%]	0.0003	2.9597 [-0.83%]	0.0004
MCTA (5 meas.)	4.6238 [0.00%]	0.0008	2.9804 [0.23%]	0.0002	2.9806 [-0.13%]	0.0003
MCTB (5 meas.)	4.6216 [-0.05%]	0.0005	2.9778 [0.15%]	0.0002	2.9769 [-0.26%]	0.0003
MCTC (5 meas.)	4.6250 [0.02%]	0.0012	2.9803 [0.23%]	0.0002	2.9807 [-0.29%]	0.0002

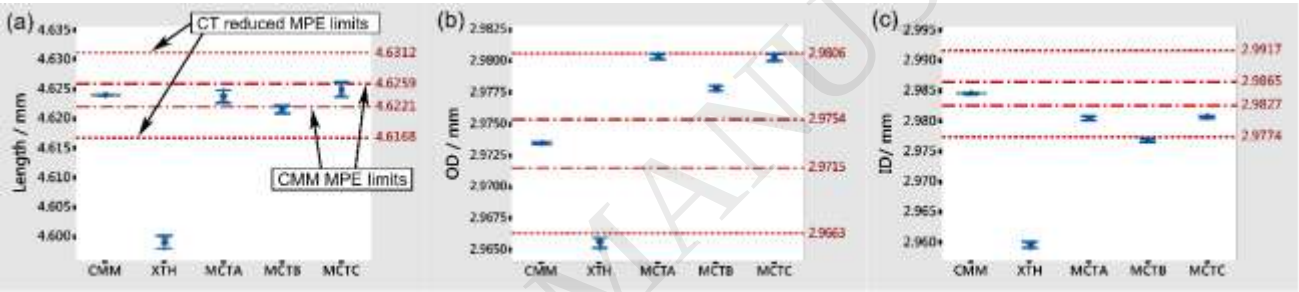

Fig. 10. Dimensional results. (a) Length, (b) Outside diameter, (c) Inside diameter.

Fig. 10 shows the measurements of Length, OD and ID of the test artefact, as measured on the CMM and the four CT machines. The confidence interval for the mean was computed at 95%. The Length values for all MCT225 metrology CT measurements are significantly within the CT manufacturer's specified MPE limits (see Fig. 10(a)). The non-metrology XT H 225 mean Length measurement was -0.54% (24.8 µm) less than the mean CMM measurement. The CT Length measurement (i.e. the step-face distance) is insensitive to surface determination errors. In contrast, the test artefact OD and ID CT measurements *are* both sensitive to surface determination errors. The percentage difference between the CT OD values and the CMM OD values are all greater (more positive) than the percentage difference between the XCT Length values and the Length CMM values. Similarly the percentage difference between the CT ID values and the CMM ID values are all less (more negative) than the percentage difference between the XCT Length values and the Length CMM values. The implication is that the surface determination algorithm, in this case, has computed the surface with additional material beyond the actual surface, toward the background (air) region for this Ti6Al4V ELI component. Material-specific differences between the computed surface and the actual surface have been noted elsewhere in the literature for other AM materials, with aluminium being computed as having too little

material and steel and ZrO_2 computed, as with the case here, additional material beyond the actual surface, using conventional surface determination methods [7].

3.2.3 Applying corrections

As discussed in 2.1.2, the dimensional test artefact used here was designed to differentiate between global voxel scaling errors and surface determination errors. Global voxel scaling errors may be corrected by using the machine manufacturer's calibrated artefacts and following a user calibration procedure (such as with the Nikon MCT225 metrology CT). Other CT machines may not be supplied with calibration artefacts, or have a specific user protocol to be followed and the machines themselves may not have a defined MPE for the measurement volume. Performing the voxel global scaling correction using the dimensional test artefact reported here is a dimensional calibration at a specific location within the machine volume, and using a material with similar X-ray attenuation properties as the AM surface test artefact permits optimising of the global voxel scaling for all machines and provides reference information about the performance of the surface determination technique used. The small dimensional test artefact, ideally, would be included in all scans of AM components that require surface extraction and analysis as the errors indicated from the dimensional analysis may guide compensation, whether for performing local voxel scaling calibration at the specific measurement site, or for optimising the surface determination techniques used, both reducing errors in the extracted surface texture data. Two mathematical corrections were applied to the extracted CT dimensional data (OD, ID and Length): a correction to compensate for global scaling errors, followed by a correction to compensate for surface determination errors. It should be noted that these mathematical scaling corrections were only applied to the extracted dimensions for the test artefact after surface determination. They were not performed during the CT volume reconstruction process and no corrections of any type were applied to any of the surface texture measurements reported here.

3.2.4 Global scaling correction

Results after performing just a global scaling correction, based on the ratio between the mean CT and CMM Length measurements, are shown in Fig. 11**Error! Reference source not found.**.

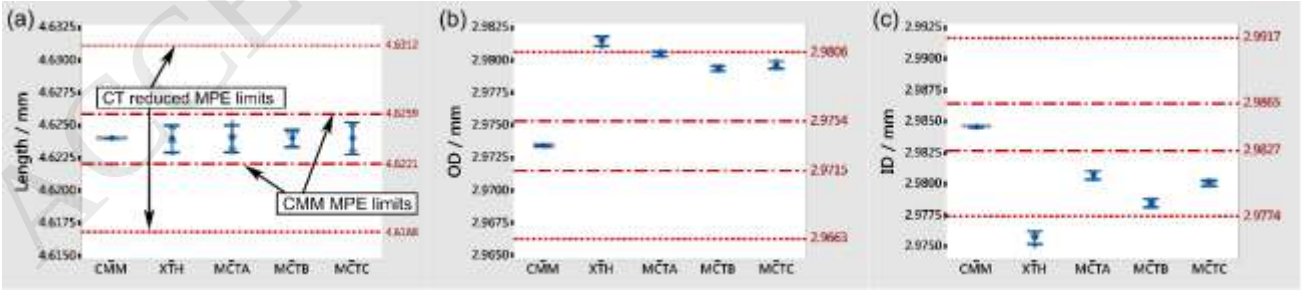

Fig. 11. Dimensional results after just global scaling correction.
(a) Length, (b) Outside diameter, (c) Inside diameter.

It can be seen that the mean Length dimensions for the CT measurements are now identical to the mean CMM measurement (see Fig. 11**Error! Reference source not found.**(a)). However, the OD and ID measurement values for the XT H 225 (XTH) exceed the metrology CT MPE limits and all values for all measurements exceed the CMM MPE limits. It can be seen that, after global scaling correction, the OD values extracted from the CT measurements are all greater than the mean CMM measurement and the ID values extracted from the CT measurements are all less than the mean CMM ID measurement. The results reported here suggest the applied surface determination computes the Ti6Al4V component oversize as the OD is greater than, and the ID is less than, the CMM mean measurements. Global scaling errors have now been compensated for so a surface determination correction factor (figuratively "removing" material) may now be applied and evaluated.

3.2.5 Global scaling followed by surface determination correction

CT surface determination computes a surface at the transition between part material and the surrounding background material. The background material for all reported measurements was air. As discussed in 3.2.2, the surface determination applied in VGStudio MAX 3.0 was computing the surface with additional material beyond the actual surface, toward the background (air) region (therefore the OD was oversize and the ID was undersize). Therefore the mathematical correction applied to the extracted dimensions should have the effect of changing the localisation of the surface by moving the surface toward the internal regions of the part (figuratively "removing" material), reducing the OD and increasing the ID. The Length is unchanged. The mathematical surface determination correction was configured to produce a similar final OD and ID percentage error. For example, the mean dimensions extracted from the MCTA measurements, after global scaling correction, were OD 2.9805 mm and ID 2.9807 mm. The mean CMM OD and ID measurements were 2.9735 mm and 2.9846 mm respectively. The difference between the CT and CMM measurements were +0.0069 mm (0.24%) for the OD and -0.0040 mm (-0.13%) for the ID. Correcting for surface determination by "removing" 0.00273 mm from the surface results in an OD of 2.9750 mm and an ID of 2.9862 mm. The difference between the CT and CMM measurements then become +0.0016 mm (0.05%) for both OD and ID. The required correction value for the surface determination error was different for all CT machines. The surface determination corrections applied are shown in Table 6. The OD and ID dimensions will change by twice the surface determination correction value.

Table 6. Surface determination correction applied to OD and ID CT data.

CT machine	Surface determination correction / µm
XTH	4.23
MCTA	2.73
MCTB	3.01
MCTC	2.67

After the mathematical global scaling correction followed by the surface determination correction the OD and ID measurements for all CT machines (including the XT H 225 industrial machine [XTH]) are not just within the MPE of the MCT225 metrology CT, but also within the MPE of the reference CMM (see Fig. 12(b,c)).

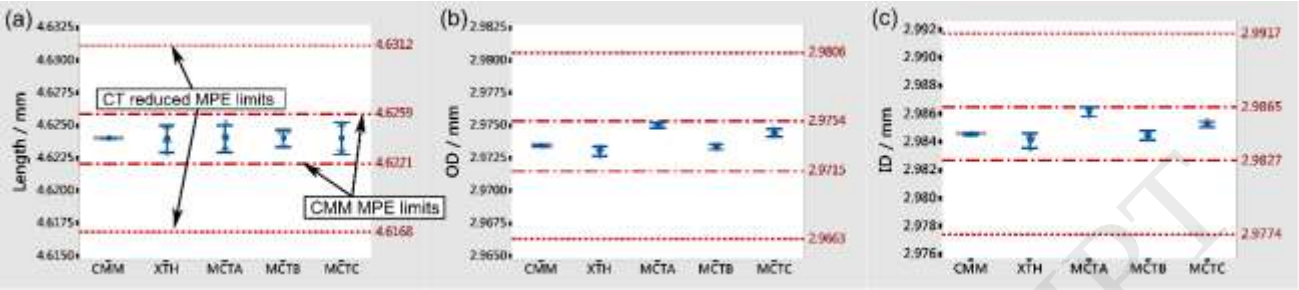

Fig. 12. Dimensional results after global scaling and surface determination correction. (a) Length, (b) Outside diameter, (c) Inside diameter.

As an illustration of the complete two-stage correction process, using the data for the XTH measurements, the mean errors in the initial un-corrected dimensions extracted from the CT measurement, with respect to (wrt) the reference CMM measurements, were: Length -24.8 µm (-0.54%), OD -8.0 µm (-0.27%) and ID -24.9 µm (-0.83%). A global surface determination correction of 1.0054 ($Length_{CMM}$ / $Length_{CT}$) was then applied to correct for the global scaling error. The mean CT OD and ID dimensions after global scaling correction were 2.9815 mm and 2.9757 mm respectively. The difference between these values and the mean CMM measurements are OD +8.0 µm (+0.27%) and ID -8.9 µm (-0.30%). If a surface determination correction of 4.23 µm is applied per surface, (figuratively "removing" material), the errors for OD and ID both become 0.0004 mm (-0.02%). The results for the XTH data are shown in Table 7. The results show, for this example, after decomposition and compensation for global scaling and surface determination errors, the residual errors an order of magnitude less than the initial errors. This error decomposition will aid in analysing AM surface extraction errors and in generating correction protocols for AM surfaces measured using CT.

Table 7. Increase in accuracy with correction steps (XT H 225 example).

Feature	CMM mean (mm)	As measured XTH (mm) [% dif. wrt CMM]	After correcting for the 0.54% global scaling error (mm) [% dif. wrt CMM]	After correcting for the global scaling error followed by surface determination correction (mm) [% dif. wrt CMM]
Length	4.6240	4.5992 **[-0.54%]**	4.6240 **[0.00%]**	4.6240 **[0.00%]**
OD	2.9735	2.9655 **[-0.27%]**	2.9815 **[+0.27%]**	2.9730 **[-0.02%]**
ID	2.9846	2.9597 **[-0.83%]**	2.9757 **[-0.30%]**	2.9841 **[-0.02%]**

3.3 The effect of measurement voxel size

The voxel size for the MCT225 measurements was 8.7 µm. The voxel size for the non-metrology XTH measurements was 17.2 µm. A single test (MCTA11.5) was performed using the metrology MCT225 used for

the MCTA measurements with the sample moved away from the X-ray source, at a magnification (source-detector distance / source-object distance) and voxel size similar to the XTH measurements. The other CT measurement parameters were unchanged (see Table 8).

Table 8. Voxel size and magnification for each measurement.

CT machine	Voxel size / µm	Magnification (source-detector distance / source-object distance)
XTH	17.2	11.5
MCTA	8.7	23
MCTA11.5	17.3	11.5

3.3.1 Surface texture results

Extracted surface texture results for the single MCTA11.5 measurement are shown in Table 9. This table also includes the values reported in Table 3 for the mean values for the FV measurements, the XTH measurements and the (8.7 µm voxel size) MCTA measurements. The difference between the CT mean values with respect to and the FV mean values are shown in Table 10. Charts for *Sa*, *Sq* and *Sz* are shown in Fig. 13.

Table 9. Surface texture results.

Parameter	Mean FV	Mean XTH	Mean MCTA	Single value MCTA11.5
Sa / µm	25.5	24.1	25.5	24.7
Sq / µm	32.6	30.9	32.5	31.6
Sz / µm	335.3	324.0	335.2	330.5
Ssk	0.26	0.08	0.20	0.10
Sku	3.7	3.7	3.6	3.7
Sdr (%)	40.2	28.3	41.9	33.0

Table 10. Differences between CT mean values and FV mean values.

Parameter	Difference between mean XCT and FV values		
	XTH	MCTA	MCTA11.5
Sa / µm	-5.2%	0.2%	-2.9%
Sq / µm	-5.2%	-0.1%	-3.0%
Sz / µm	-3.4%	0.0%	-1.4%
Ssk (absolute)	-0.2	-0.1	-0.2
Sku	-2.0%	-2.9%	-2.5%
Sdr (%) (absolute)	-12.0	1.7	-7.2

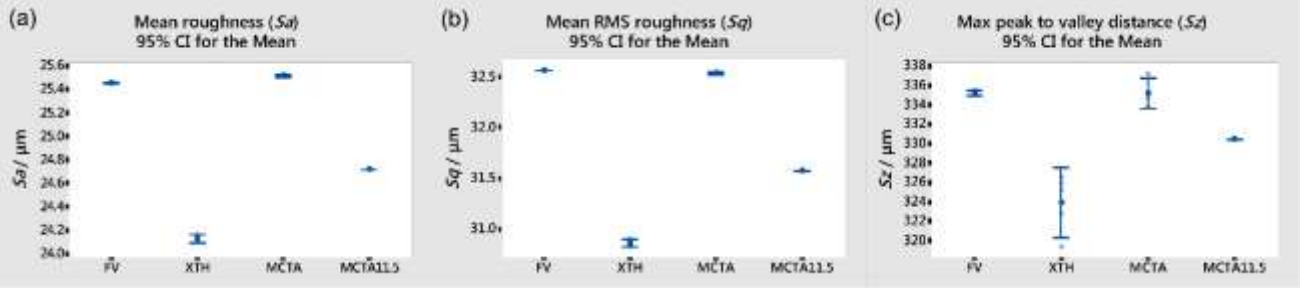

Fig. 13. Surface texture results for CMM, XTH, MCTA and MCTA11.5. (a) *Sa*, (b) *Sq*, (c) *Sz*.

The values of *Sa*, *Sq* and *Sz* for the MCTA11.5 measurement were significantly lower than those obtained with the smaller voxel size obtained with the initial higher magnification measurement on the same machine. The values were, however, not comparable to the XTH measurements even though the voxel size was similar: it can be seen that the difference between the XTH and FV measurement values was approximately twice the difference between the MCTA11.5 values and the FV values. The lower XTH results are due a combination of factors, including the scaling error present in the XTH measurements: the XTH mean Length (from the dimensional measurement) is 0.54% undersize (see Table 5). It is considered that a global scaling reduction will result in lower surface texture parameters such as *Sa* and *Sq* [15].

A further test was performed to investigate the maximum measurement voxel size that would still produce sufficient information for correct surface characterisation. The ALSi10Mg aluminium AM test artefact reported in [15], together with the Ti6Al4V ELI test artefact used in the work reported here were measured on the XT H 225 machine. The test artefacts were scanned at the voxel size used for the RR measurements (17.3 µm) and then positioned progressively further away from the X-ray source to increase voxel size and reduce magnification. The surface data was extracted and filtered using the same filtering employed for the other measurements: 8 mm L-filter nesting index and 0.025 mm S-filter nesting index. The results are shown in Fig. 14.

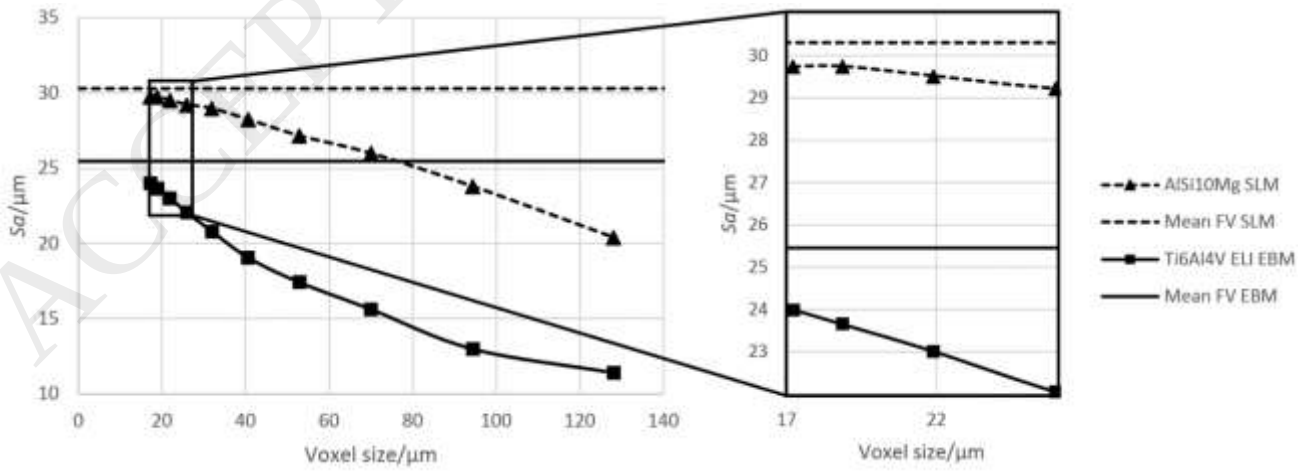

Fig. 14. *Sa* vs voxel size, XT H 225 CT.

The mean values of the FV measurements are also shown on the graphs. It can be seen that the trace for the ALSi10Mg AM sample is approximately horizontal between voxel sizes of 19 µm and 17 µm. This shows the voxel size is sufficiently small that a reduction in voxel size will not significantly change the value of the extracted *Sa* value. However, it can be seen that the trace for the Ti6Al4V ELI sample used in the RR has not become horizontal by 17.3 µm. This indicates that the magnification and resolution of the XT H 225 CT measurements of the RR test artefact may not have been sufficiently high to characterise the surface. These initial results indicate, as a guide, that for a typical as-built AM surface the voxel size for full characterisation should be less than one half the surface *Sa* value. This information will be used to modify the measurements recommended for the Stage 2 RR.

3.3.2 Dimensional results

The Length dimension extracted from the single MCTA11.5 measurement matched the CMM mean Length measurement (4.624 mm) (see Fig. 15), so no global scaling correction was required. To optimise the CT dimensional measurements required a 4.33 µm surface determination correction, similar to the 4.23 µm correction applied to the XTH measurements and more than the 2.73 µm correction applied to the ×23 magnification MCTA measurements. Once this correction was applied the difference between the single MCTA11.5 OD and ID measurements and the mean CMM measurements were less than 0.005% (less than 0.2 µm).

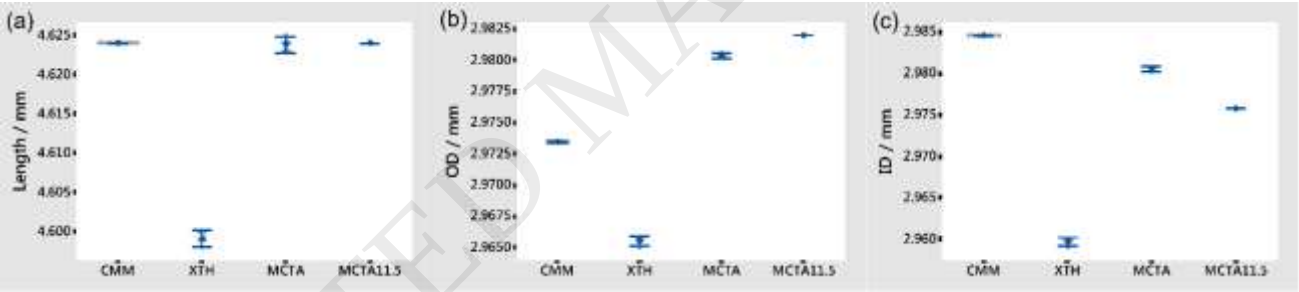

Fig. 15. Dimensional results for the CMM, XTH, MCTA and MCTA11.5.
(a) Length, (b) Outside diameter, (c) Inside diameter.

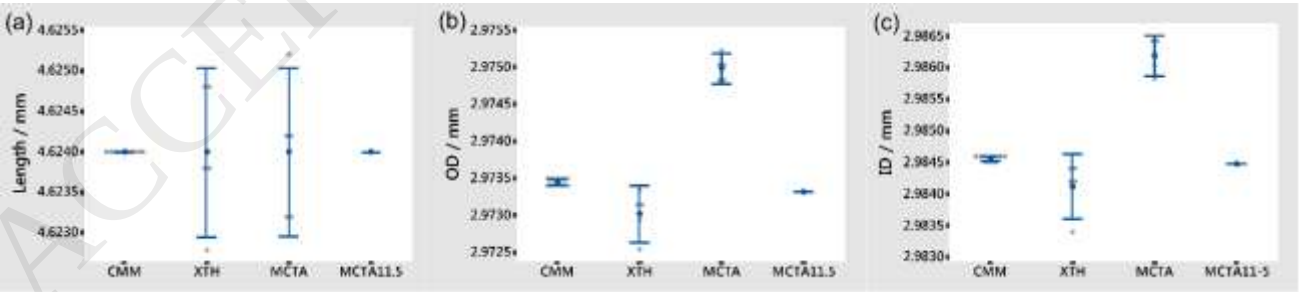

Fig. 16. Dimensional results after global scaling and surface determination mathematical correction.
(a) Length, (b) Outside diameter, (c) Inside diameter.

4 Conclusions

The results from a four-participant interlaboratory comparison investigating the extraction of ISO 25178-2 areal surface texture data from X-ray CT measurements have been reported. Results show the robustness of the extraction and analysis process reported in [15] and confirm the validity of using CT for the extraction of surface texture data from additively manufactured parts. As an example, the value of *Sa* for all metrology CTs was within 0.5% of the mean reference measurement obtained using FV. There was good repeatability and reproducibility of all measurement results. Baseline results provide a good knowledge grounding for an expanded Stage 2 CT-STARR interlaboratory comparison. It is expected that Stage 2 will include measurements of several metal AM surface texture artefacts, manufactured using electron beam and laser systems, with extraction and evaluation performed on several artefact surfaces. A reference dimensional test artefact, manufactured from a similar material to the AM test artefact, was included in all CT measurements. This artefact was shown to differentiate between global voxel scaling errors and surface determination errors. Once the error types were separated mathematical correction was performed for both error types. The combination of surface determination and scaling correction resulted in dimensional numbers very similar to reference CMM measurements. For example, the test artefact errors for the XT H 225 commercial CT for Length, OD and ID reduced from -0.27%, -0.83% and -0.54% respectively to all < 0.02%. Using a dimensional test artefact during the CT measurement of AM surfaces provides good process validation and should be invaluable during the second stage of this RR. Planned future work includes the generation of correction algorithms to correct the extracted surface texture data based on the dimensional test artefact surface determination and global scaling results. Factors affecting the accuracy of the results have been discussed, such as surface determination, measurement voxel size and number of projections. Further investigation of these factors will be conducted to ascertain their influence on measurement accuracy, so as to create a recommended measurement and analysis envelope within which to work for optimised surface-from-CT results.

Acknowledgements

A. Townsend, R. Racasan and L. Blunt gratefully acknowledge the UK's Engineering and Physical Sciences Research Council (EPSRC) funding of the EPSRC Future Metrology Hub (Grant Ref: EP/P006930/1). A. Thompson and R.K. Leach would like to thank EPSRC (Grants EP/M008983/1 and EP/L01534X/1) and 3TRPD Ltd. for funding this work. N. Senin and R.K. Leach would also like to thank the EC-FP7-PEOPLE-MC METROSURF for supporting this work.

References

[1] A. Thompson, I. Maskery, R.K. Leach, X-ray computed tomography for additive manufacturing: a review, Measurement Science and Technology 27(7) (2016) 072001.
[2] W.W. Wits, S. Carmignato, F. Zanini, T.H. Vaneker, Porosity testing methods for the quality assessment of selective laser melted parts, CIRP annals 65(1) (2016) 201-204.
[3] P. Iassonov, T. Gebrenegus, M. Tuller, Segmentation of X-ray computed tomography images of porous materials: A crucial step for characterization and quantitative analysis of pore structures, Water Resources Research 45(9) (2009).
[4] S. Tammas-Williams, H. Zhao, F. Léonard, F. Derguti, I. Todd, P. Prangnell, XCT analysis of the influence of melt strategies on defect population in Ti–6Al–4V components manufactured by Selective Electron Beam Melting, Materials Characterization 102 (2015) 47-61.
[5] S. Khademzadeh, F. Zanini, P.F. Bariani, S. Carmignato, Precision additive manufacturing of NiTi parts using micro direct metal deposition, The International Journal of Advanced Manufacturing Technology 96(9) (2018) 3729-3736.
[6] S.L. Sing, S. Wang, S. Agarwala, F.E. Wiria, T.M.H. Ha, W.Y. Yeong, Fabrication of titanium based biphasic scaffold using selective laser melting and collagen immersion, (2017).
[7] J.P. Kruth, M. Bartscher, S. Carmignato, R. Schmitt, L. De Chiffre, A. Weckenmann, Computed tomography for dimensional metrology, CIRP Annals-Manufacturing Technology 60(2) (2011) 821-842.
[8] S. Carmignato, Accuracy of industrial computed tomography measurements: experimental results from an international comparison, CIRP Annals-Manufacturing Technology 61(1) (2012) 491-494.
[9] K. Kiekens, F. Welkenhuyzen, Y. Tan, B. Ph, A. Voet, J.P. Kruth, W. Dewulf, A test object with parallel grooves for calibration and accuracy assessment of industrial computed tomography (CT) metrology, Measurement Science and Technology 22(11) (2011) 115502.
[10] G. Kerckhofs, G. Pyka, M. Moesen, S. Van Bael, J. Schrooten, M. Wevers, High-Resolution Microfocus X-Ray Computed Tomography for 3D Surface Roughness Measurements of Additive Manufactured Porous Materials, Advanced Engineering Materials 15(3) (2013) 153-158.
[11] G. Pyka, G. Kerckhofs, I. Papantoniou, M. Speirs, J. Schrooten, M. Wevers, Surface Roughness and Morphology Customization of Additive Manufactured Open Porous Ti6Al4V Structures, Materials 6(10) (2013) 4737-4757.
[12] A. Thompson, N. Senin, R.K. Leach, Towards an additive surface atlas, Proceedings of dimensional accuracy and surface finish in additive manufacturing, ASPE 2016 Summer Topical Meeting, Raleigh, NC, 2016, pp. 156-161.
[13] A. Townsend, N. Senin, L. Blunt, R.K. Leach, J.S. Taylor, Surface texture metrology for metal additive manufacturing: a review, Precision Engineering 46 (2016) 34-47.
[14] ISO 25178-2, Geometrical product specifications (GPS) Surface texture: Areal - Part 2: Terms, definitions and surface texture parameters, ISO, 2012.
[15] A. Townsend, L. Pagani, P. Scott, L. Blunt, Areal surface texture data extraction from X-ray computed tomography reconstructions of metal additively manufactured parts, Precision Engineering 48(Supplement C) (2017) 254-264.
[16] N. Senin, A. Thompson, R.K. Leach, Characterisation of the topography of metal additive surface features with different measurement technologies, Measurement Science and Technology 28(9) (2017) 095003.
[17] A. Thompson, N. Senin, C. Giusca, R. Leach, Topography of selectively laser melted surfaces: A comparison of different measurement methods, CIRP Annals-Manufacturing Technology (2017).
[18] A. Townsend, R. Racasan, P. Bills, L. Blunt, Development of an interlaboratory comparison investigating the generation of areal surface texture data per ISO 25178 from XCT, 7th conference on industrial computed tomography, Leuven, Belgium, 2017.
[19] ISO 4288, Geometric product specification (GPS) Surface texture. Profile method: Rules and procedures for the assessment of surface texture, ISO, 1998.
[20] ISO 25178-3, Geometrical product specifications (GPS) Surface texture: Areal Part 3: Specification operators, ISO, 2012.
[21] V. Aloisi, S. Carmignato, Influence of surface roughness on X-ray computed tomography dimensional measurements of additive manufactured parts, Case studies in nondestructive testing and evaluation 6 (2016) 104-110.
[22] A. Triantaphyllou, C.L. Giusca, G.D. Macaulay, F. Roerig, M. Hoebel, R.K. Leach, B. Tomita, K.A. Milne, Surface texture measurement for additive manufacturing, Surface Topography: Metrology and Properties 3(2) (2015) 024002.

[23] G. Krolczyk, P. Raos, S. Legutko, Experimental analysis of surface roughness and surface texture of machined and fused deposition modelled parts, Tehnički Vjesnik-Technical Gazette 21 (2014) 217-221.
[24] S. Carmignato, W. Dewulf, R.K. Leach, Introduction to industrial X-ray computed tomography, Springer2017.
[25] Nikon metrology NV, Nikon CT Pro 3D.
[26] Volume Graphics GmbH, VGStudio MAX.
[27] Visual Computing Lab - ISTI - CNR, Meshlab. http://meshlab.sourceforge.net/.
[28] CloudCompare (version 2.6.3beta) [GPL software] 2015. www.danielgm.net. (Accessed 2015.
[29] The MathWorks, Inc., Natick, Mass, USA, Matlab Release R2015b.
[30] NPL, Softgages for the evaluation of profile surface texture parameters, 2005. http://resource.npl.co.uk/softgauges/Help.htm#sdf.
[31] U.o.H. The Centre for Precision Technologies, SurfStand.
[32] Keyence, Tolerance and measurement accuracy, 2017. https://www.keyence.com/ss/products/measure/measurement_library/basic/tolerance/. 2017).